JOURNAL OF AIRCRAFT
Vol. 35, No. 5, September–October 1998

Aerodynamic Design of Transonic Wings Using the Target Pressure Optimization Approach

Hyoung-Jin Kim* and Oh-Hyun Rho†
Seoul National University, Seoul 151-742, Republic of Korea

A target pressure optimization code with a genetic algorithm was developed for the inverse design of transonic wings. The shock strength was minimized, and the isobar line sweep angles on the upper surface of the wing were maximized to obtain minimum wave drag while constraints on spanwise lift distribution and section pitching moments were satisfied. With the target pressures at each design section specified, an inverse design code was run subsequently to obtain the wing geometry. The designed wing showed better performance than the baseline wing at the given design condition, and geometrical constraints on the section contour area are successfully satisfied. Design results show that the inverse design using the target pressure optimization approach was very efficient in obtaining a transonic wing of high performance at a given design condition.

Nomenclature

A	=	normalized wing section area, area/c^2
C_L, C_D, C_{Dw}, C_M	=	wing lift, drag, wave drag, and moment coefficient
C_l, C_d, C_{dw}, C_m	=	section lift, drag, wave drag, and moment coefficient
C_{pt}, C_{pc}	=	target and computed pressure coefficient
c	=	wing section chord
ds	=	design section
M, M_∞	=	local, freestream Mach number
t/c	=	maximum thickness-to-chord ratio of wing section
η	=	semispan fraction, $2y/b$
$\Lambda_{L.E.}$	=	sweep angle of leading edge
$\Lambda_{1/2}$	=	sweep angle of 1.2 chord line

Subscripts

i	=	index of wing section surface grid points
0	=	value of the baseline wing

Introduction

WITH the advances in computational fluid dynamics, computational design methods in the aerodynamic design of aircraft components have become even more important than before. Computational methods in aerodynamic design can be roughly categorized into the following two classes: 1) direct numerical optimization methods and 2) inverse methods. The inverse methods are much faster and more efficient than the direct numerical optimization. However, it is not so easy to specify a target pressure distribution, which renders favorable aerodynamic performance and reasonable shape. Although a skillful aerodynamic designer can come up with successful target pressures, design efficiency can be improved by providing the designers with a tool for specifying the target pressure.

For this purpose, numerical optimization of the target pressure for the inverse design of transonic airfoils has been studied by several researchers.[1–3] Obayashi and Takanashi,[2] in particular, also conducted a three-dimensional wing design with the target pressure optimization approach. However, they optimized target pressures in a two-dimensional manner and imposed the same target pressure at each of the design sections. They did not consider any three-dimensional features such as planform, shock sweep angle, spanwise wing loading, etc.

Some other strategies were also exploited to circumvent the difficulty in imposing target pressures. Campbell[4,5] developed the constrained direct iterative surface curvature (CDISC) method to avoid the difficulty of target pressures specification, and applied it to the design of airfoils and wings. The CDISC method develops initial target pressure distributions from the current analysis pressure and then modifies them in the design process to meet the desired flow characteristics. Jameson et al.[6] adopted a two-stage design strategy for a design of a wing–body transport aircraft. In the first stage a design calculation is performed in the direct optimization mode with Euler equations. Then in the second stage the pressure distributions of the Euler solution are used as the target pressures for inverse design with the Navier–Stokes equations.

In this study the optimization of target pressures for transonic transport wing designs is emphasized and, thus, a target pressure optimization code for transonic wing design is developed and applied for transonic transport wing design problems. Three-dimensional features such as spanwise wing loading distribution and shock sweep angles or isobar line sweep angles as well as section lift and moment coefficients are considered, and compressibility drag is minimized for given constraints. A genetic algorithm (GA) is adopted to optimize target pressures as in the two-dimensional target pressure optimization case.[3] The optimized target pressures can be used as input data to any kinds of inverse design codes that are applicable to three-dimensional transonic wing design. The hybrid inverse optimization method developed by Santos and Sankar[7] is used for inverse design of transonic wings. This paper will present details of the procedure used in the inverse design routine, target pressure optimization, and some design examples.

Flow Analysis

A three-dimensional Navier–Stokes solver developed by Hwang[8] is used for flow analysis. Reynolds-averaged three-dimensional compressible thin-layer Navier–Stokes equations are used in conservation form. Roe's flux difference splitting

Received Nov. 10, 1997; presented as Paper 98-0599 at the AIAA 36th Aerospace Sciences Meeting, Reno, NV, Jan. 12–15, 1998; revision received March 22, 1998; accepted for publication April 15, 1998.

*Graduate Research Assistant, Department of Aerospace Engineering. Student Member AIAA.

†Professor, Department of Aerospace Engineering. Senior Member AIAA.

scheme is adopted for the space discretization; a MUSCL approach with flux limiter is employed to obtain a higher order of accuracy. Yoon and Jameson's lower-upper symmetric-Gauss–Seidel method is used in the implicit part. Turbulence effects are considered using the Baldwin–Lomax model with relaxation technique. To improve convergence, local time stepping is applied.

A C-type grid system around the section airfoil is generated by a conformal mapping technique and expanded spanwisely to produce a C–O-type grid system. We use 135 points in the streamwise direction, 41 points in the normal direction, and 30 points in the spanwise direction.

The transonic flow over the ONERA M6 wing is analyzed to validate this flow solver and grid system. The flow condition is $M_\infty = 0.84$, $\alpha = 3.06$ deg, and $Re_\infty = 11 \times 10^6$ based on the semispan length. The pressure distributions along the two spanwise stations of the wing are displayed in Fig. 1. The present results agree well with the experimental data.[9] The lift and drag coefficients are compared with another computation[10] as the experimental values are not known (see Table 1). Although a somewhat coarser grid has been used here, the lift and drag coefficients agree well with the fine grid result (289 × 65 × 49).

Table 1 Comparison of aerodynamic coefficients of ONERA M6 wing[a]

	C_L	C_D
Present result (135 × 41 × 30)	0.2695	0.01817
Radespiel et al.[10] (289 × 65 × 49)	0.2677	0.01782

[a] $M_\infty = 0.84$, $\alpha = 3.06$ deg, and $Re_\infty = 11 \times 10^6$.

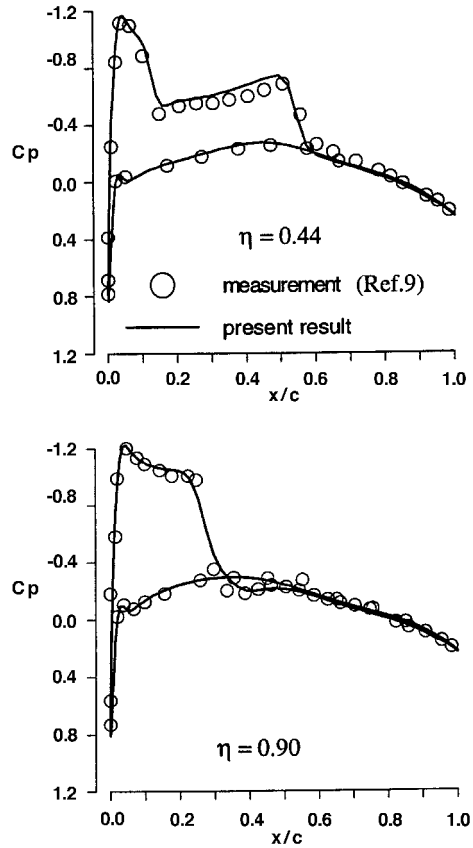

Fig. 1 Pressure distribution for ONERA M6 wing ($M_\infty = 0.84$, $\alpha = 3.06$ deg, and $Re_\infty = 11 \times 10^6$).

Hybrid Inverse Optimization Method

The modified Garabedian–McFadden (MGM) equation[11] is used to correlate the difference between the computed surface pressure and the target pressure to modify the wing section geometry

$$F_0 \Delta z + F_1 \Delta z_x + F_2 \Delta z_{xx} = R, \qquad (R = C_{pt} - C_{pc}) \quad (1)$$

where coefficients F_0, F_1, and F_2 are nonnegative constants chosen to provide a stable iterative process, and R is the residual. The MGM equation is solved using a finite difference scheme. The discretized MGM equation forms a tridiagonal system and can be written as

$$[M]\{\overline{\Delta z}\} = \{R\} \quad (2)$$

The detailed expressions for elements of matrix M are given by Malone et al.[11]

The objective function is defined to solve Eq. (2) with an optimization technique as follows:

$$F(\overline{\Delta z}) = \tfrac{1}{2} \left| [M]\{\overline{\Delta z}\} - \{R\} \right|^2 \quad (3)$$

An external penalty function method is used to specify the geometric constraint. The conjugate gradient method[12] is utilized to minimize the objective function [Eq. (3)]. The computational time required to calculate the objective function and its derivative is negligible compared with the time required by the flow solver. The geometry of the design section is updated by adding the displacement Δz_i to the corresponding grid points.

The preceding method was developed by Santos and Sankar[7] and is referred to as the "hybrid inverse optimization method" because it solves the inverse design problem with an optimization technique.

Target Pressure Optimization with a GA

A target pressure optimization code developed by the authors for the optimization of target pressures for transonic airfoil inverse design has been extended for three-dimensional wing design.[3] Figure 2 shows the characteristic surface pressure distribution defined by eight points for a typical transonic wing section. Shape functions are used for interpolation between these points. The location of characteristic points, local Mach number at each point, and the coefficients of shape functions are used as design variables. The boundary-layer calculation is avoided to reduce computational time. Instead, the slope of the pressure distribution is checked as the flow separation criteria. Some details of the target pressure optimization are explained next.

Definition of Shape Functions (Refer to Fig. 2)

Stagnation flow region (4 ~ 3, 4 ~ 5): In the two-dimensional case we used a stagnation flow shape function,[1] defined

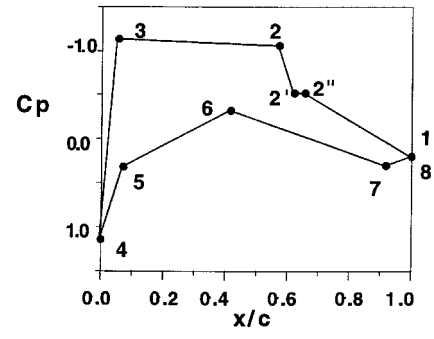

Fig. 2 Schematic representation of target pressure.

by approximating the potential flow velocity distribution around elliptic cylinders (for small x/c and small incidence angle)

$$\left.\frac{u}{u_\infty}\right|_{2D} = \frac{(1 + da_1)\sqrt{da_3 \times (x/c)} \pm [da_2 + da_3 \times da_4 \times (x/c)]\sqrt{1 - da_3 \times (x/c)}}{\sqrt{da_3 \times (x/c) + \frac{1}{4}da_1^2}} \tag{4}$$

$+$ sign for upper surface and $-$ for lower surface. $da_1 \sim da_4$ represent the design variables that should be adjusted in the optimization procedure. Nose radius and incidence angle may be estimated from the following equations:

$$(R/c)_{\text{nose}} = (0.5/da_3) \times da_1^2(1 - M_\infty^2)$$

$$\alpha = da_2 \times \sqrt{(1 - M_\infty^2)}, \text{ rad}$$

Unlike the two-dimensional flow around the airfoil, the value of u_4 is not zero but $u_\infty \sin \Lambda_{\text{L.E.}}$ by simple sweep theory. Thus, some modification is made to Eq. (4) as follows:

$$\left.\frac{u}{u_\infty}\right|_{\text{sweep}} = \frac{u_4}{u_\infty} + \left(1 - \frac{u_4}{u_3}\right)\left.\frac{u}{u_\infty}\right|_{2D} \tag{5}$$

Roof-top region ($3 \sim 2$, $5 \sim 6$):

$$M = db_1 + db_2[(x/c) - (x/c)_{b_0}]^{1+db_3} \tag{6}$$

Index b_0 refers to the starting point of the region.

Shock relation ($2 \sim 2'$): In the two-dimensional cases, shock was specified when M exceeded 1.1 at control point 2.[3] Here, the shock-triggering Mach number is $1.1/\cos \Lambda_{1/2}$ by the simple sweep theory. The shock thickness value, which is defined as the difference between the chordwise location of point 2 and $2'$, is set to $0.05c$. In viscous airfoil flow, the pressure jump measured at the foot of the shock is less than the Rankine–Hugoniot pressure jump. Thus, a modified Rankine–Hugoniot relation of the following form is used for an approximation of the pressure jump[13]:

$$\frac{p_{2'}}{p_2} = 1 + \frac{2\gamma}{\gamma + 1}A(M_2^2 - 1), \qquad 0.55 \le A \le 0.75 \tag{7}$$

A is set to 0.65 for this case.

Constant pressure region behind shock ($2' \sim 2''$): It is known that a pressure plateau behind the shock wave is necessary to stabilize the boundary layer.[14] A constant pressure distribution is specified for length l, l being the design variable. However, it is not intended to stabilize the boundary layer by varying the length l.

Pressure recovery region on upper surface ($2'' \sim 1$): This region could be represented by an approximating function of Stratford pressure distribution. However, a straight line connecting the two points is used for simplicity. C_p at the trailing edge are given a priori.

Pressure recovery region on lower surface ($6 \sim 7$): A fourth-order polynomial is defined for this region as

$$M = M_6 + dc_1\left(\frac{x}{c} - \frac{x_6}{c}\right) + dc_2\left(\frac{x}{c} - \frac{x_6}{c}\right)^2 + dc_3\left(\frac{x}{c} - \frac{x_6}{c}\right)^3 + dc_4\left(\frac{x}{c} - \frac{x_6}{c}\right)^4 \tag{8}$$

Rear loading region ($7 \sim 8$): For this region a simple polynomial is defined as

$$M = M_7 + dd_1\left(\frac{x}{c} - \frac{x_7}{c}\right) + dd_2\left(\frac{x}{c} - \frac{x_7}{c}\right)^2 \tag{9}$$

Characteristic points and shape functions presented in the preceding text can represent target pressure distribution around the transonic wing section. Not all of them are independent and 15 design variables per each design section were used for target pressure optimization. In this study three design sections were used, making the number of design variables 45.

Estimation of Wing Characteristics

Before the aerodynamic coefficients are estimated, the pressure distribution is smoothed in the following manner:

$$Cp_{i,\text{new}} = w \times Cp_i + \frac{1 - w}{2}(Cp_{i-1} - Cp_{i+1}) \qquad 0 < w < 1 \tag{10}$$

It is assumed that wing sections with the same value of the following equation at the same flow condition, planform, and spanwise position have the same maximum thickness[1]:

$$\left(\frac{t}{c}\right) \cong -\frac{\sqrt{1 - M_\infty^2}}{2}\int_0^1 \frac{Cp_u + Cp_l}{2}\,\mathrm{d}\left(\frac{x}{c}\right) \tag{11}$$

A relation to estimate the magnitude of wave drag coefficient of an airfoil has been proposed by Campbell[4]:

$$C_{\text{dw}} \cong \frac{0.04}{(t/c)^{1.5}}(M_2 - 1)^4 \tag{12}$$

The wave drag coefficient of a sweep back wing section is approximated as follows:

$$C_{\text{dw}} \cong \frac{0.04}{(t/c)^{1.5}}\left(M_2 \cos \theta_s - \frac{1.1}{\cos \Lambda_{1/2}} + 0.1\right)^4 \tag{13}$$

where θ_s is the shock sweep angle. An estimation of the total wave drag coefficient of a wing can be obtained by integrating the section values along the wingspan:

$$C_{\text{Dw}} \cong \frac{2}{S}\int_0^{b/2} C_{\text{dw}} c \times \mathrm{d}y \tag{14}$$

We can reduce the wave drag by reducing M_2, the Mach number in front of the shock wave and $\cos \theta_s$.

To consider the viscous drag component the boundary-layer calculation can be included in the target optimization code at the cost of additional computational time. However, the inclusion of viscous drag has little effect on the optimum solution because the increment of compressibility drag is dominant in the total increment of wing drag in transonic flow region, and flow separation can be prevented by specifying a constraint on the slope of the pressure distribution. If this target pressure optimization method is to be applied to subsonic airfoil/wing design, boundary-layer calculation should be included.

Problem Definition

The objective of optimization in this study is to obtain target pressures that render less wave drag than the baseline wing with lift, with maximum thickness being nearly the same. The wing loading is specified as an elliptic distribution to reduce

the induced drag. The optimization problem is defined as follows.

Minimize C_{Dw} subject to 1) elliptic wing loading distribution, 2) $t_0/c - 0.001 \le t/c \le t_0/c + 0.001$, 3) $C_{m0} - 0.02 \le C_m \le C_{m0} + 0.02$, and 4) $dC_p/d(x/c) \le 2.3$.

Constraint 4 on the gradient of the pressure is taken from Ref. 14 to avoid flow separation after the shock and is specified for the pressure recovery region. Some other constraints were also imposed to make the target pressure distribution reasonable: 5) $0.4 \le Cp_7 \le Cp_8$, 6) $Cp|_{x/c=0.2} \le 0$, 7) $Cp|_{x/c=0.6} \le 0$, and 8) $-0.4 \le Cp_6 \le 0$ (where the subscripts are the control point numbers in Fig. 2). Constraint 5 is employed to make the pressure distribution rear-loaded and is not specified on the inboard design section. In this study an additional constraint is also specified such that the pressure distribution on the lower surface and around the leading edge is similar to that of the baseline wing.

All of the constraints were specified at each design section and included in the objective function as the penalty function term multiplied by proper weighting factors. Although only the section moment constraint is roughly specified here, a constraint on the total moment coefficient C_M can also be specified.

Optimization with GA

The objective function of this target pressure optimization problem is severely nonlinear, and the gradient of the objective function is discontinuous.[1] Thus a robust optimization technique that does not use the gradient information of the objective function should be used. GA is a searching algorithm based on natural selection and survival of the fittest. It has become popular recently because of its robustness and capability for finding the global minimum.

In this study the Genocop code (version 2.1), which adopts a GA based on the real number coding, is applied for the target pressure optimization.[15] In the Genocop code reproduction is based on the cumulative probability of survival of each population. The agents that died are replaced by a new population generated by seven genetic operators: whole arithmetic crossover, simple arithmetic crossover, heuristic crossover, uniform mutation, boundary mutation, nonuniform mutation, and whole nonuniform mutation. The frequencies of the seven operators are set equal.

Figure 3 shows a flowchart of target pressure optimization by GA. First, populations are randomly created, then a pressure distribution is made for each population, lift and moment coefficients are calculated, and drag coefficient and maximum thickness are estimated. With these values, fitness values can be calculated for each population. Genetic operators such as reproduction, crossovers, and mutations are applied to generate new populations of the next generation. This routine is repeated until the maximum generation number is reached.

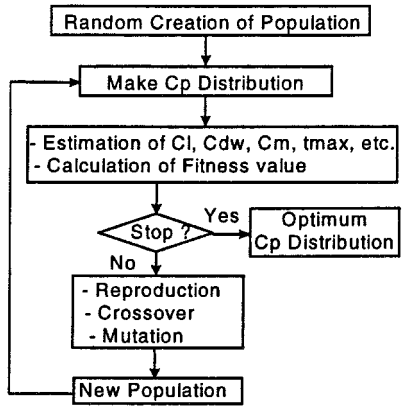

Fig. 3 Flow chart of target pressure optimization.

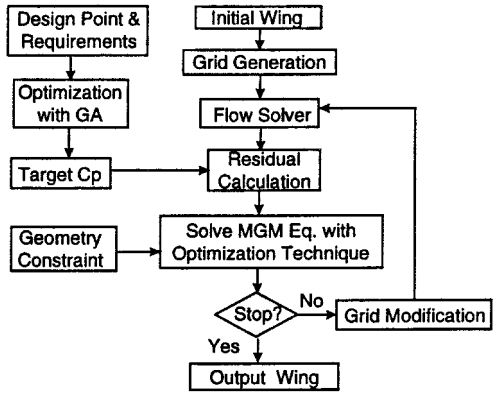

Fig. 4 Flow chart of inverse wing design.

Design Procedure

The flowchart of a transonic wing design routine is shown in Fig. 4. First, a baseline wing is selected and a grid system is generated around the wing. The surface pressure is obtained by the flow solver at a given design condition. Target pressure is optimized with GA for the given flow condition and constraints. Then the hybrid inverse optimization method is used to obtain the vertical displacements of the design section grid points reducing the objective function [Eq. (3)] and satisfying the geometric constraints. Design sections are updated with the vertical displacements. Wing sections other than the design sections are interpolated from the design sections by a C-spline method inboard and by a linear interpolation outboard. Then the grid system is modified algebraically for the new wing geometry. This design cycle is repeated until the geometric modification is sufficiently small.

Results and Discussion

The sweep angle of the baseline wing is 27 deg, and the aspect ratio is 8.49. The chord length ratio of the wing tip to the root is 0.266, and that of the wing planform break position to the root is 0.58. The wing section at the outer board is RAE2822, and the section airfoil at the root is the uncambered RAE2822. The thickness-to-chord ratio of the section airfoil is increased to 15% at the root and reduced to 11% at the break and tip. The C-spine interpolation is used to generate inboard sections and linear interpolation for outboard sections. The twist angle is 4 deg. Three design sections are selected as $\eta = 0.057$, 0.343, and 0.918. The second design section is at the wing planform break position.

Design Example I

Design conditions are $M_\infty = 0.78$, $C_L = 0.50$, and $Re = 7 \times 10^6$, based on the root chord length. The objective of the first design example is to improve the performance of the baseline wing at the given flow condition.

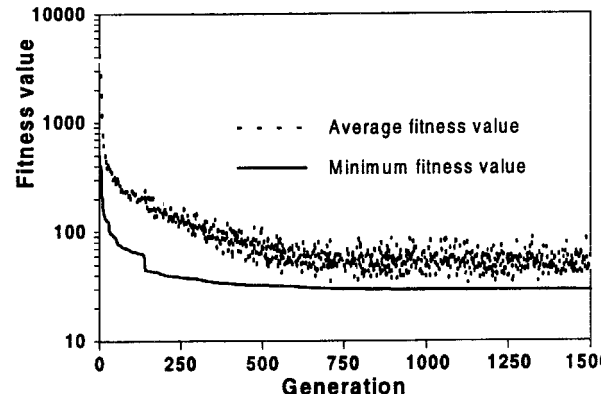

Fig. 5 Evolution history of populations.

First, the flowfield around the baseline wing is analyzed to obtain the surface pressure distribution and the aerodynamic coefficients. Then the target pressure at the design condition is optimized. GA was run with the population number of 200 and maximum generation number of 1500. Figure 5 shows the evolution history of population. Because of severe nonlinearity of the objective function, some populations with very large fitness value occur in almost every generation throughout the evolution process. Thus, the average fitness value does not decrease after the 500th generation and keeps oscillating. Computational time for target optimization with GA was about 30 min using a Pentium personal computer running at 120 MHz. A population number of 400 was also tested to obtain nearly the same optimum solution.

With the optimized target pressure at each design section, an inverse design was performed to produce subsequent wing geometry. Geometric constraints are specified on design section areas as follows:

$$0.0900 \leq A_{ds1} \leq 0.0920$$

$$0.0708 \leq A_{ds2} \leq 0.0720 \qquad (15)$$

$$0.0708 \leq A_{ds3} \leq 0.0720$$

where lower limits of the inequality equations are the normalized section contour areas of the baseline wing.

It took about 1.5 times the cost of an analysis to run the inverse design code. The designed wing will be referred to as W7850, which represents a wing designed at $M_\infty = 0.78$ and $C_L = 0.50$.

Figure 6 shows the pressure distribution and wing section shape at each design section, a reduction of shock strength can be seen. Also, the location of shock has been moved upstream in the neighborhood of the root (design section 1) and downstream in the neighborhood of the tip (design section 3). Consequently, the shock sweep angle has been increased.

Although the target pressure on the lower surface was thought to be similar to that of the baseline, the target pressure at design section 1 is very different from the baseline pressure. This caused a drastic change in the section airfoil shape. The first design section airfoil of W7850 had a flatter upper surface and a smaller nose radius than the baseline, and the camber was increased at the front part of the section airfoil. The second design section airfoil was slightly changed to remove the shock wave. The section airfoil of design section 3 had a smaller nose radius than the baseline. Figure 7 shows the upper surface pressure contour of the baseline wing and W7850. The shock strength is reduced and the shock sweep angle is increased.

In Table 2 the aerodynamic performance has been improved, and the geometric constraint on the section contour area has been satisfied. The section contour areas all have the upper limit values of the given constraint [Eq. (15)]. Figure 8 shows the wing loading distribution over the wingspan. The wing loading distribution of W7850 compares well with the target elliptic wing loading distribution.

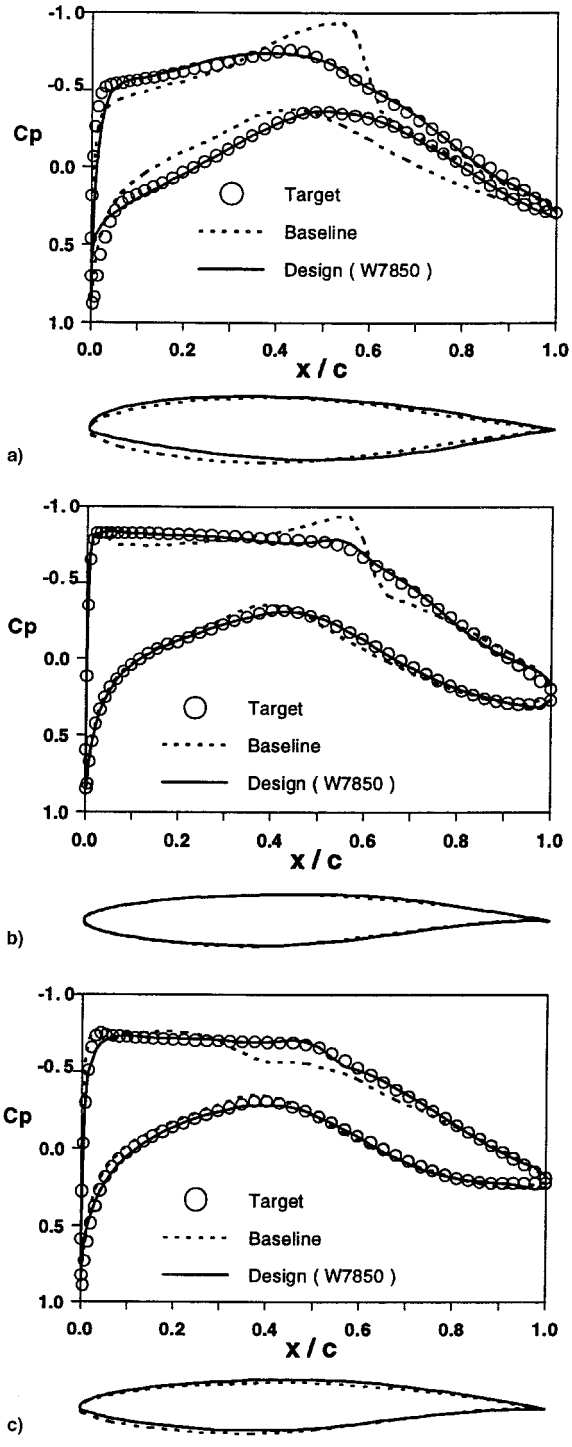

Fig. 6 Surface pressure and airfoil shape at $C_L = 0.50$. Design section a) 1 ($\eta = 0.057$), b) 2 ($\eta = 0.343$), and c) 3 ($\eta = 0.918$).

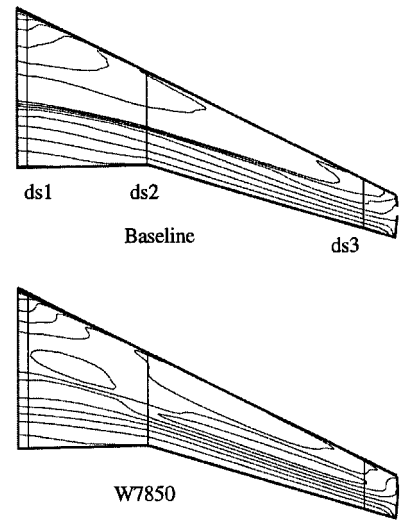

Fig. 7 Upper surface pressure contours at $C_L = 0.50$.

Table 2 Aerodynamic coefficients of example I

	Baseline	W7850	Δ, %
C_L	0.4973	0.4989	+0.22
C_D	0.02167	0.02088	−3.65
L/D	22.94	23.89	+4.14
A			
$ds1$	0.0900	0.0920	+2.22
$ds2$	0.0708	0.0720	+1.69
$ds3$	0.0708	0.0720	+1.69

Table 3 Aerodynamic coefficients of example II

	W7850	W7860	Δ, %
C_L	0.5939	0.5985	+0.77
C_D	0.02635	0.02591	−1.67
L/D	22.54	23.10	+2.48
A			
$ds1$	0.0920	0.0900	−2.22
$ds2$	0.0720	0.0720	0
$ds3$	0.0720	0.0719	−0.14

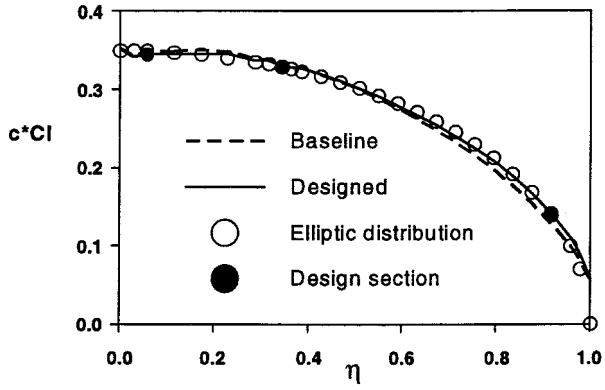

Fig. 8 Wing loading distribution at $C_L = 0.50$.

Design Example II

The objective of the second design example is to improve the off-design performance of W7850 when the lift coefficient is increased by 0.1. The design condition is $C_L = 0.60$ with other conditions; this is the same as the first design example. The angle of incidence is increased to obtain a lift coefficient of 0.60. The target pressure was optimized with the same population and generation number as design example I. The inverse code was run with the same geometric constraint [Eq. (15)]. It also took about 1.5 times the cost of an analysis to run the inverse design code as in the first design example. The designed wing will be referred to as W7860, which represents a wing designed at $M_\infty = 0.78$ and $C_L = 0.60$. Figure 9 shows the pressure distribution and the wing section shape at each design section. As in example I, shock strength has been reduced. Also, shock sweep angle has been increased by moving the shock upstream in the neighborhood of the root (design section 1) and downstream in the neighborhood of the tip (design section 3). The first design section airfoil of W7860 has a flatter upper surface and a larger nose radius than W7850. For the second design section airfoil, slight change has been observed near the 70% chord to remove the weak shock. The third design section airfoil has a sharper leading edge than W7850.

Figure 10 shows the upper surface pressure contour of W7850 and W7860 at $C_L = 0.60$. W7860 has larger sweep angles of isobar lines than W7850, and the shock strength at the design sections is decreased. However, shock wave still exists at the midregion of outboard. To improve this design result the number of design sections should be increased. Although it is not shown here, the wing loading distribution over the wingspan compared well with the target elliptic distribution. Table 3 shows aerodynamic coefficients of W7850 and W7860. W7860 has better performance than W7850 at $C_L = 0.60$.

The off-design performance of the wings designed through the two design examples is shown in Fig. 11. When C_L is around 0.50, W7850 has a larger L/D value, whereas W7860 has a larger L/D value at higher lift coefficients. This shows the limit of single-point design; single-point design does not guarantee its off-design performance. Therefore, multipoint de-

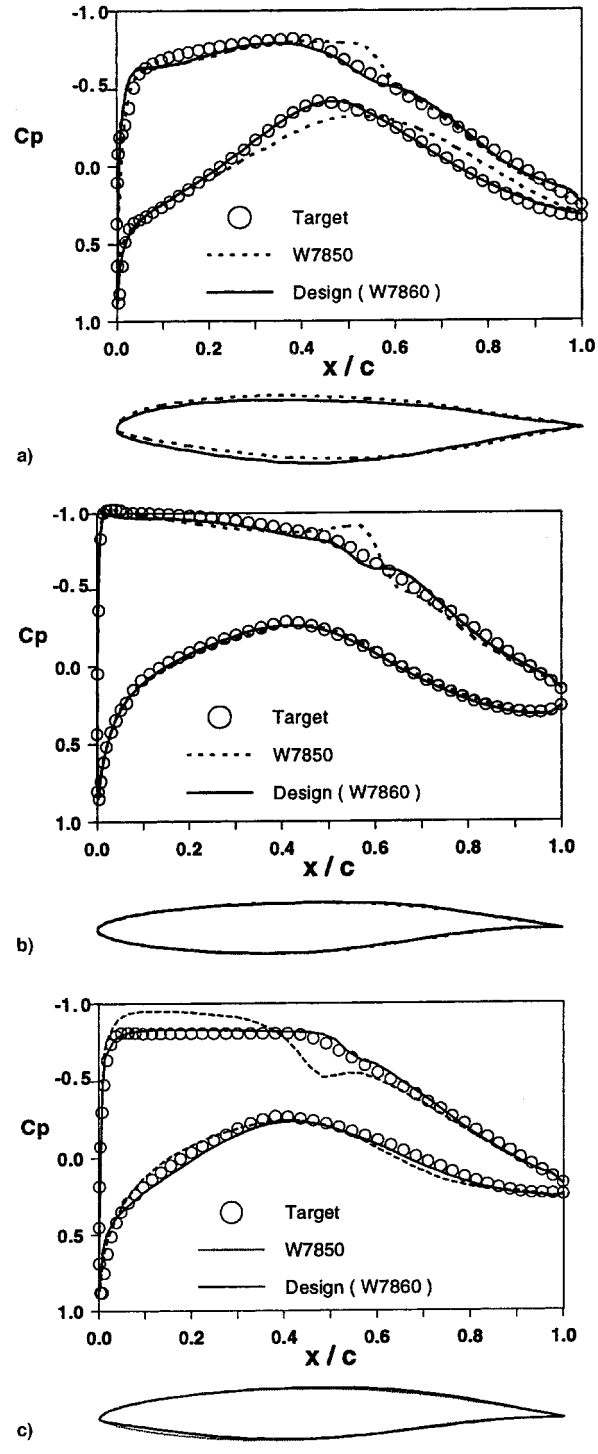

Fig. 9 Surface pressure and airfoil shape at $C_L = 0.60$. Design section a) 1 ($\eta = 0.057$), b) 2 ($\eta = 0.343$), and c) 3 ($\eta = 0.918$).

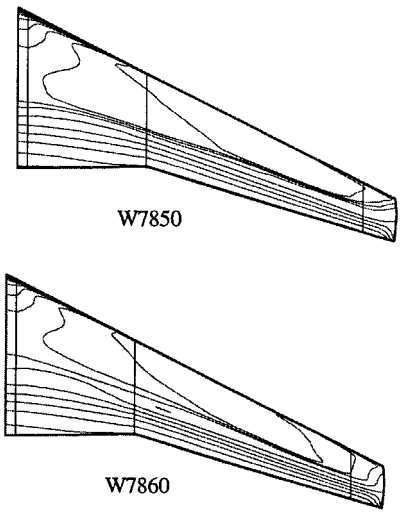

Fig. 10 Upper surface pressure contours at $C_L = 0.60$.

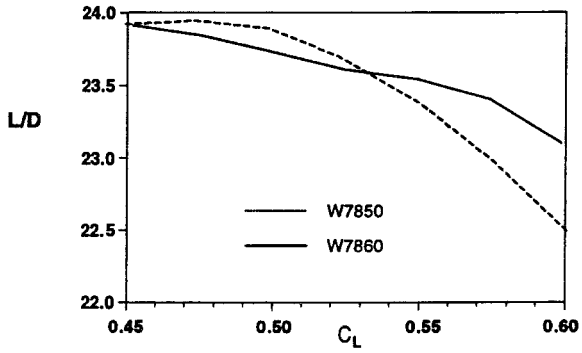

Fig. 11 C_L vs L/D curves.

sign is needed to improve the off-design performance of single-point design.

Concluding Remarks

A target pressure optimization code with GA has been developed for transonic wing design problems. The inverse design of transonic wings has been performed by the hybrid inverse optimization method with the optimized target pressures. The single-point designed wings showed better performance than the initial wings at the design condition. The designed wings have a weaker shock and a larger shock sweep angle than the initial wings. By utilizing this target pressure optimization code, the transonic wing design could be performed very efficiently.

To improve the quality of the optimum target pressure, shape functions for the target pressure optimization should be refined, and the number of control points and shape functions should be increased. To consider viscous drag component, boundary-layer calculation should be included in the target optimization code with the cost of computation time. In addition, the number of design sections should be increased to further improve single-point design.

Also, multipoint design is required to improve off-design performance. The extension of this design approach to multipoint transonic wing design is underway.

Acknowledgment

The authors would like to acknowledge the financial support from Systems Engineering Research Institute Supercomputer Center through the Cray R&D Grant Program.

References

[1]Van Egmond, J. A., "Numerical Optimization of Target Pressure Distributions for Subsonic and Transonic Airfoil Design," *Computational Methods for Aerodynamic Design (Inverse) and Optimization*, AGARD, CP 463, March 1990 (Ref. 17).

[2]Obayashi, S., and Takanashi, S., "Genetic Optimization of Target Pressure Distribution for Inverse Design Methods," AIAA Paper 95-1649, June 1995.

[3]Kim, H. J., and Rho, O.-H., "Dual-Point Design of Transonic Airfoils Using the Hybrid Inverse Optimization Method," *Journal of Aircraft*, Vol. 34, No. 5, 1997, pp. 612–618.

[4]Campbell, R. L., "An Approach to Constrained Aerodynamic Design with Application to Airfoils," NASA TP-3260, Sept. 1992.

[5]Campbell, R. L., "Efficient Constrained Design Using Navier-Stokes Codes," AIAA Paper 95-1808, June 1995.

[6]Jameson, A., Pierce, N. A., and Martinelli, L., "Optimum Aerodynamic Design Using the Navier-Stokes Equations," AIAA Paper 97-0101, Jan. 1997.

[7]Santos, L. C., and Sankar, L. N., "A Hybrid Inverse Optimization Method for the Aerodynamic Design of Lifting Surfaces," AIAA Paper 94-1895, June 1994.

[8]Hwang, S. W., "Numerical Analysis of Unsteady Supersonic Flow over Double Cavity," Ph.D. Dissertation, Seoul National Univ., Seoul, Republic of Korea, Feb. 1996.

[9]Schmitt, V., and Charpin, F., "Pressure Distribution on the ONERA M6 Wing at Transonic Mach Numbers," AGARD-AR-138, May 1979.

[10]Radespiel, R., Rossow, C., and Swanson, R. C., "Efficient Cell-Vertex Multigrid Schemes for the Three-Dimensional Navier-Stokes Equations," *AIAA Journal*, Vol 28, No. 8, 1990, pp. 1464–1472.

[11]Malone, J. B., Narramore, J. C., and Sankar, L. N., "Airfoil Design Method Using the Navier-Stokes Equations," *Journal of Aircraft*, Vol. 28, No. 3, 1991, pp. 216–224.

[12]Press, W. H., Teukolsky, S. A., Vetterling, W. T., and Flannery, B. P., "Numerical Recipes in FORTRAN," 2nd ed., Cambridge Univ. Press, Cambridge, England, UK, 1992, pp. 413–418.

[13]Mabey, D. G., "Physical Phenomena Associated with Unsteady Transonic Flows," *Unsteady Transonic Aerodynamics*, edited by D. Nixon, Vol. 120, Progress in Astronautics and Aeronautics, AIAA, New York, 1989, pp. 1–55.

[14]Harris, C. D., "NASA Supercritical Airfoils—A Matrix of Family-Related Airfoils," NASA TP-2969, March 1990.

[15]Michalewicz, Z., *Genetic Algorithms + Data Structures = Evolution Programs*, Springer–Verlag, New York, 1992.